


## Dispersive determination of fourth generation quark masses

Hsiang-nan Li 

*Institute of Physics, Academia Sinica, Taipei, Taiwan 115, Republic of China*



(Received 8 October 2023; accepted 31 May 2024; published 24 June 2024)

We determine the masses of the sequential fourth generation quarks  $b'$  and  $t'$  in the extension of the Standard Model by solving the dispersion relations associated with the mixing between the neutral states  $Q\bar{q}$  and  $\bar{Q}q$ , with  $Q$  ( $q$ ) being a heavy (light) quark. The box diagrams responsible for the mixing, which provide the perturbative inputs to the dispersion relations, involve multiple intermediate channels, i.e., the  $ut$  and  $ct$  channels,  $u$  ( $c$ ,  $t$ ) being an up (charm, top) quark, in the  $b'$  case, and the  $db'$ ,  $sb'$ , and  $bb'$  ones,  $d$  ( $s$ ,  $b$ ) being a down (strange, bottom) quark, in the  $t'$  case. The common solutions for the above channels lead to the masses  $m_{b'} = (2.7 \pm 0.1)$  and  $m_{t'} \approx 200$  TeV unambiguously. We show that these superheavy quarks, forming bound states in a Yukawa potential, barely contribute to Higgs boson production via gluon fusion and decay to photon pairs and bypass current experimental constraints. The mass of the  $\bar{b}'b'$  ground state is estimated to be about 3.2 TeV. It is thus worthwhile to continue the search for  $b'$  quarks or  $\bar{b}'b'$  resonances at the (high-luminosity) Large Hadron Collider.

DOI: [10.1103/PhysRevD.109.115024](https://doi.org/10.1103/PhysRevD.109.115024)

### I. INTRODUCTION

Our recent dispersive analyses of some representative physical observables (heavy meson decay widths, neutral meson mixing, etc.) have accumulated substantial indications that the scalar sector of the Standard Model (SM) is not completely free, but arranged properly to achieve internal dynamical consistency [1–3]. Fermion masses can be derived by solving the dispersive relations for decay widths of a heavy quark  $Q$  as an inverse problem [4–7]: starting with massless final-state up and down quarks, we demonstrated that the solution for the  $Q \rightarrow d\bar{u}$  ( $Q \rightarrow c\bar{u}$ ) mode with the leading-order heavy-quark-expansion input yields the charm-quark (bottom-quark) mass  $m_c = 1.35$  ( $m_b = 4.0$ ) GeV [1]. Requiring that the dispersion relation for the  $Q \rightarrow s\bar{u}$  ( $Q \rightarrow d\mu^+\nu_\mu$ ,  $Q \rightarrow u\tau^-\bar{\nu}_\tau$ ) decay generates the identical heavy-quark mass, we deduced the strange-quark (muon,  $\tau$  lepton) mass  $m_s = 0.12$  GeV ( $m_\mu = 0.11$ ,  $m_\tau = 2.0$  GeV). The similar studies of fermion mixing [3] established the connections between the Cabibbo-Kobayashi-Maskawa (CKM) matrix elements and quark masses and between the Pontecorvo-Maki-Nakagawa-Sakata matrix elements and neutrino masses. These connections explained the known numerical relation  $V_{us} \approx \sqrt{m_s/m_b}$  [8],  $V_{us}$  being a CKM matrix element, and

the maximal mixing angle  $\theta_{23} \approx 45^\circ$  in the lepton sector and discriminated the normal hierarchy for neutrino masses from the inverted hierarchy or quasidegenerate spectrum.

The dispersion relation for the correlation function of two  $b$ -quark scalar (vector) currents, with the perturbative input from the  $b$ -quark loop, returns the Higgs ( $Z$ ) boson mass 114 (90.8) GeV [2] in accordance with the measured values. It implies that the parameters  $\mu^2$  and  $\lambda$  in the Higgs potential are also constrained by internal dynamical consistency. Particle masses and mixing angles in the SM originate from the independent elements of the Yukawa matrices [9], as the electroweak symmetry is broken. Inspired by the above observations, we attempt to make a bold conjecture that the SM contains only three fundamental parameters actually, i.e., the three gauge couplings, and the other parameters, governing the interplay among various generations of fermions, are fixed by SM dynamics itself. The analyticity, which is inherent in quantum field theories, imposes additional constraints. Its impact is not revealed in naive parameter counting at the Lagrangian level based on symmetries, but through dispersive analyses of dynamical processes. Dispersion relations, which physical observables like heavy-to-light decay widths must respect, link different types of interactions at arbitrary scales. The resultant constraints are so strong that the parameters in the scalar sector must take specific values, instead of being discretionary.

To maintain the simplicity and beauty conjectured above, a natural extension of the SM is to introduce the sequential fourth generation of fermions, since the associated parameters in the scalar sector are not free. That is, their masses and mixing with lighter generations can be predicted

*Published by the American Physical Society under the terms of the Creative Commons Attribution 4.0 International license. Further distribution of this work must maintain attribution to the author(s) and the published article's title, journal citation, and DOI. Funded by SCOAP<sup>3</sup>.*

unambiguously in a similar manner [2]. We first determine the top-quark mass  $m_t$  by solving the dispersion relations for the mixing between the neutral states  $Q\bar{u}$  and  $\bar{Q}u$ . The perturbative inputs to the dispersion relations come from the imaginary contributions of the box diagrams for the mixing with the intermediate  $db$ ,  $sb$ , and  $bb$  channels. Given the corresponding thresholds  $m_d + m_b$ ,  $m_s + m_b$ , and  $2m_b$  for the typical quark masses  $m_d = 0$ ,  $m_s = 0.1$  GeV, and  $m_b = (4.15 \pm 0.01)$  GeV, we extract  $m_t = (173 \pm 3)$  GeV from the common solution to the three channels. The existence of such a common solution is highly nontrivial, making convincing our formalism and predictions obtained from it. We then go ahead to calculate the masses of the sequential fourth generation quarks  $b'$  and  $t'$  in the same framework, considering the multiple intermediate channels  $ut$  and  $ct$  in the  $b'$  case, and  $db'$ ,  $sb'$ , and  $bb'$  in the  $t'$  case. It will be observed that the common solutions for the various channels also exist and demand the masses  $m_{b'} = (2.7 \pm 0.1)$  and  $m_{t'} \approx 200$  TeV.

Many merits of the sequential fourth generation model have been explored: condensates of the fourth generation quarks and leptons could be the responsible mechanism of the dynamical electroweak symmetry breaking [10,11]; electroweak baryogenesis through the first-order phase transition could be realized in this model [12]; it could provide a viable source of  $CP$  violation for the baryon asymmetry of the Universe based on the dimensional analysis of the Jarlskog invariants [13]. However, it is widely conceded that this model has been ruled out mainly by the data of Higgs boson production via gluon fusion  $gg \rightarrow H$  and decay into photon pairs  $H \rightarrow \gamma\gamma$  [14]. Measurements of the oblique parameters, which depend on the additional mixing angles associated with the fourth generation quarks and the unclear contribution from the fourth generation leptons [15], give relatively weaker constraints. We point out that the superheavy fourth generation quarks  $b'$  and  $t'$  with the aforementioned masses form bound states in a Yukawa potential [16,17]. Once they form bound states, physical degrees of freedom change and new resonances emerge, so one has to reformulate the interaction between the fourth generation quarks and Higgs bosons with these new resonances [18]. We will show that the  $\bar{b}'b'$  scalars contribute to the  $gg \rightarrow H$  cross section only at  $10^{-3}$  level, relative to that from the top-quark loop in the SM. It is thus likely for the sequential fourth generation model to bypass the current experimental constraints, even without the expansion of the scalar sector [19]. For an analogous reason, the model could also bypass the constraint from Higgs boson decay to photon pairs.

The rest of the paper is organized as follows. We compute the top-quark mass from the dispersion relations for the  $Q\bar{u}$  and  $\bar{Q}u$  mixing through the  $db$ ,  $sb$ , and  $bb$  channels in Sec. II. The framework is extended to the prediction for the  $b'$  ( $t'$ ) quark mass in Sec. III by investigating the multiple intermediate  $ut$  and  $ct$  ( $db'$ ,  $sb'$ , and  $bb'$ ) channels. The properties

of the  $\bar{b}'b'$  scalar bound states  $S$  in a Yukawa potential, including the binding energies and the widths, are derived in Sec. IV, based on which we estimate the  $gg \rightarrow S \rightarrow H$  cross sections using the  $ggS$  and  $SH$  effective couplings and Breit-Wigner propagators for  $S$ . In particular, the mass of the  $\bar{b}'b'$  ground state, being either a pseudoscalar or a vector, is evaluated in a relativistic approach and found to be about 3.2 TeV. Some processes, which are promising for searching for  $b'$  quarks and their resonances at the (high-luminosity) Large Hadron Collider, are proposed. Section V contains the summary.

## II. FORMALISM AND TOP-QUARK MASS

Consider the mixing between the neutral states  $Q\bar{u}$  and  $\bar{Q}u$  through the box diagrams with a heavy quark  $Q$  of mass  $m_Q$  and a massless  $u$  quark [2,20]. The construction of a dispersion relation follows the procedure in [1] straightforwardly, which starts with the contour integration of the mixing amplitudes  $\Pi_{ij}$ ,  $ij = db, sb$ , and  $bb$ , in the complex  $m$  plane. The contour consists of two pieces of horizontal lines above and below the branch cut along the positive real axis, two pieces of horizontal lines above and below the branch cut along the negative real axis, a small circle around the pole  $m = m_Q$  located on the positive real axis, and a circle  $C_R$  of large radius  $R$  as depicted in Fig. 1. As recollected in the Appendix, we have the dispersion relations for the imaginary pieces of  $\Pi_{ij}$

$$\int_{M_{ij}^2}^{R^2} \frac{\text{Im}\Pi_{ij}(m)}{m_Q^2 - m^2} dm^2 = \int_{m_{ij}^{\text{box}}}{R^2} \frac{\text{Im}\Pi_{ij}^{\text{box}}(m)}{m_Q^2 - m^2} dm^2. \quad (1)$$

The quark-level thresholds  $m_{ij}$  for the box-diagram contributions  $\text{Im}\Pi_{ij}^{\text{box}}$  denote  $m_i + m_j$ , i.e.,  $m_{db} = m_d + m_b$ ,  $m_{sb} = m_s + m_b$ , and  $m_{bb} = 2m_b$ . The physical quantities  $\text{Im}\Pi_{ij}(m)$  on the left-hand side of the above expression have the hadronic thresholds  $M_{db} = m_\pi + m_B$ ,  $M_{sb} = m_K + m_B$ , and  $M_{bb} = 2m_B$  with the pion (kaon,  $B$ -meson)

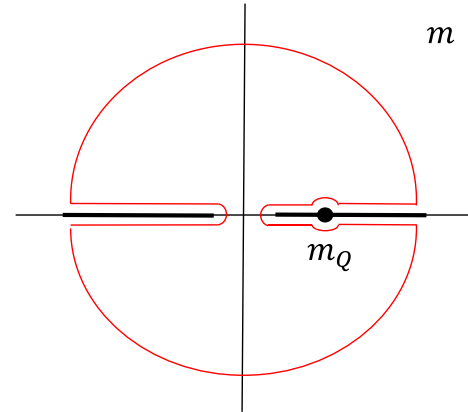


FIG. 1. Contour for the derivation of Eq. (1), where the thick lines represent the branch cuts.

mass  $m_\pi$  ( $m_K, m_B$ ). The CKM factors associated with the  $db$ ,  $sb$ , and  $bb$  channels can vary independently in a mathematical viewpoint, so their corresponding dispersion relations can be analyzed separately. These dispersion relations, holding for arbitrary  $m_Q$ , impose stringent connections between high- and low-mass behaviors of the mixing amplitudes.

The box diagrams generate two effective four-fermion operators of the  $(V-A)(V-A)$  and  $(S-P)(S-P)$  structures. Viewing that the two structures endow separate dispersion relations, and the latter also receives contributions from amplitudes other than the box diagrams, like the double penguin amplitude [21], we concentrate on the former. The imaginary piece of the  $(V-A)(V-A)$  structure in perturbative evaluations [22,23] is written as

$$\begin{aligned} \Gamma_{ij}^{\text{box}}(m_Q) &\propto \frac{C_2^2(m_Q) \sqrt{[m_Q^2 - (m_i + m_j)^2][m_Q^2 - (m_i - m_j)^2]}}{m_Q^4 (m_W^2 - m_i^2)(m_W^2 - m_j^2)} \\ &\times \left\{ 2 \left( m_W^4 + \frac{m_i^2 m_j^2}{4} \right) [m_Q^2 - (m_i + m_j)^2] \right. \\ &\times [m_Q^2 - (m_i - m_j)^2] \\ &\left. - 3m_W^2 m_Q^2 (m_i^2 + m_j^2)(m_Q^2 - m_i^2 - m_j^2) \right\}, \quad (2) \end{aligned}$$

with the  $W$ -boson mass  $m_W$  and the intermediate quark masses  $m_i$  and  $m_j$ . A  $d$  quark is also treated as a massless particle, i.e.,  $m_d = 0$ . The overall coefficient, irrelevant to the derivation below, is implicit. We have kept only the Wilson coefficient  $C_2(\mu)$  [24], which dominates over  $C_1(\mu)$  at the renormalization scale  $\mu = m_Q \geq m_b$ . The second term in the curly brackets of Eq. (2) is down by a tiny ratio  $(m_i^2 + m_j^2)/m_W^2$ , so the behavior of Eq. (2) in  $m_Q$  is dictated by the first term. In the threshold regions with  $m_Q \sim m_{ij}$ , it is approximated by

$$\begin{aligned} \Gamma_{db}^{\text{box}}(m_Q) &\sim \frac{(m_Q^2 - m_b^2)^3}{m_Q^4}, \\ \Gamma_{sb}^{\text{box}}(m_Q) &\sim \frac{\sqrt{[m_Q^2 - (m_b + m_s)^2][m_Q^2 - (m_b - m_s)^2]}^3}{m_Q^4}, \\ \Gamma_{bb}^{\text{box}}(m_Q) &\sim \frac{\sqrt{m_Q^2 - 4m_b^2}^3}{m_Q}. \quad (3) \end{aligned}$$

Because of  $m_s \ll m_b$ ,  $m_b - m_s$  is not very distinct from  $m_b + m_s$ , and the dependence on the former has been retained in the second line of Eq. (3).

Motivated by the above threshold behaviors, we choose the integrands for the dispersion integrals in Eq. (1) as [2]

$$\begin{aligned} \text{Im}\Pi_{db}(m) &= \frac{m^4 \Gamma_{db}(m)}{(m^2 - m_b^2)^2}, \\ \text{Im}\Pi_{sb}(m) &= \frac{m^4 \Gamma_{sb}(m)}{[m^2 - (m_b + m_s)^2]^2 \sqrt{m^2 - (m_b - m_s)^2}^3}, \\ \text{Im}\Pi_{bb}(m) &= \frac{m \Gamma_{bb}(m)}{m^2 - 4m_b^2}, \quad (4) \end{aligned}$$

where  $\Gamma_{ij}(m)$  are the unknowns to be solved for shortly, and the definitions of  $\text{Im}\Pi_{ij}^{\text{box}}(m)$  by means of  $\Gamma_{ij}^{\text{box}}(m)$  should be self-evident. Note that  $\Gamma_{bb}^{\text{box}}(m)$  is an odd function in  $m$ , which accounts for the odd power of  $m$  in the numerator of  $\text{Im}\Pi_{bb}(m)$  [2]. The above integrands with powers of  $m$  in the numerators suppress any residues in the low- $m$  region, including those from the poles at  $m = \pm(m_i + m_j)$  and  $m = \pm(m_i - m_j)$ , compared to the ones from  $m = \pm m_Q$  at large  $m_Q$ . The denominators alleviate the divergent behaviors caused by the modified numerators at large  $m$ . The factor  $\sqrt{m^2 - (m_b - m_s)^2}$  in  $\Pi_{sb}(m)$  introduces an additional branch cut along the real axis in the interval  $-(m_b - m_s) < m < m_b - m_s$  in the  $m$  plane. Our contour crosses the real axis between  $m = -(m_b + m_s)$  and  $m = -(m_b - m_s)$  and between  $m = m_b - m_s$  and  $m = m_b + m_s$  and runs along the real axis marked by  $m < -(m_b + m_s)$  and  $m > m_b + m_s$ , such that this additional branch cut does not contribute.

Moving the integrands on the right-hand side of Eq. (1) to the left-hand side, we arrive at

$$\int_{m_{ij}^2}^{\infty} \frac{\Delta\rho_{ij}(m)}{m_Q^2 - m^2} dm^2 = 0, \quad (5)$$

with the subtracted unknown functions  $\Delta\rho_{ij}(m) \equiv \text{Im}\Pi_{ij}(m) - \text{Im}\Pi_{ij}^{\text{box}}(m)$ . Owing to the subtraction of the box-diagram contributions and the limits  $\text{Im}\Pi_{ij}(m) \rightarrow \text{Im}\Pi_{ij}^{\text{box}}(m)$  at large  $m$ , the integrals in Eq. (5) converge even after the upper bound of  $m^2$  is extended to infinity. The unknowns  $\Delta\rho_{ij}(m)$  are fixed to the initial conditions  $-\text{Im}\Pi_{ij}^{\text{box}}(m)$  in the interval  $(m_{ij}, M_{ij})$  of  $m$ , in which the physical quantities  $\text{Im}\Pi_{ij}(m)$  vanish. The idea behind our formalism is similar to that of QCD sum rules [25], but with power corrections in  $(M_{ij} - m_{ij})/m_Q$  arising from the difference between the quark-level and hadronic thresholds, which are necessary for establishing a physical solution [20]. As seen later, it is easier to solve for  $\Delta\rho_{ij}(m_Q)$  than for  $\Delta\Gamma_{ij}(m_Q) \equiv \Gamma_{ij}(m_Q) - \Gamma_{ij}^{\text{box}}(m_Q)$ , because the initial conditions of the former are simpler. Once  $\Delta\rho_{ij}(m_Q)$  are attained, we convert them to  $\Delta\Gamma_{ij}(m_Q)$  following Eq. (4). Without the power corrections, i.e., if  $m_{ij}$  are equal to  $M_{ij}$ , there will be only the trivial solutions  $\Delta\Gamma_{ij}(m_Q) = 0$ , i.e.,  $\Gamma_{ij}(m_Q) = \Gamma_{ij}^{\text{box}}(m_Q)$  and no constraint on the top-quark mass.

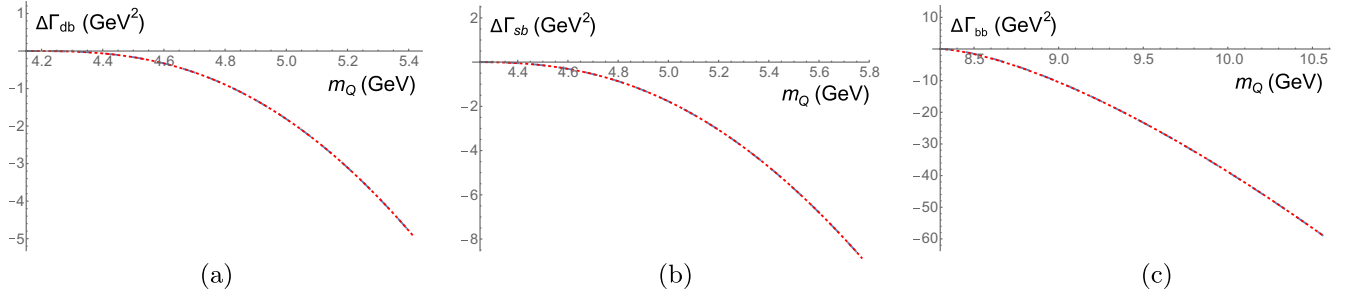


FIG. 2. Comparison of  $\Delta\Gamma_{ij}(m_Q) \equiv \Gamma_{ij}(m_Q) - \Gamma_{ij}^{\text{box}}(m_Q)$  from the fit (dotted line) with the input  $-\Gamma_{ij}^{\text{box}}(m_Q)$  (dashed line) in the interval  $(m_{ij}, M_{ij})$  of  $m_Q$  for (a)  $ij = db$ , (b)  $ij = sb$ , and (c)  $ij = bb$ .

The steps of solving Eq. (5) have been elucidated in [1] and briefly reviewed in the Appendix. The solution of the unknown function can be constructed with a single Bessel function of the first kind  $J_\alpha(x)$ ,

$$\Delta\rho_{ij}(m_Q) \approx y_{ij} \left( \omega \sqrt{m_Q^2 - (m_i + m_j)^2} \right)^{\alpha_{ij}} \times J_{\alpha_{ij}} \left( 2\omega \sqrt{m_Q^2 - (m_i + m_j)^2} \right). \quad (6)$$

A solution to the dispersion relation must not be sensitive to the arbitrary scale  $\omega$ , which results from scaling the integration variable  $m^2$  in Eq. (5) artificially [2]. To realize this insensitivity, we make a Taylor expansion of  $\Delta\rho_{ij}(m_Q)$ ,

$$\Delta\rho_{ij}(m_Q) = \Delta\rho_{ij}(m_Q)|_{\omega=\bar{\omega}_{ij}} + \frac{d\Delta\rho_{ij}(m_Q)}{d\omega} \Big|_{\omega=\bar{\omega}_{ij}} \times (\omega - \bar{\omega}_{ij}) + \frac{1}{2} \frac{d^2\Delta\rho_{ij}(m_Q)}{d\omega^2} \Big|_{\omega=\bar{\omega}_{ij}} \times (\omega - \bar{\omega}_{ij})^2 + \dots, \quad (7)$$

where the constant  $\bar{\omega}_{ij}$ , together with the index  $\alpha_{ij}$  and the coefficient  $y_{ij}$ , are fixed through the fit of the first term  $\Delta\rho_{ij}(m_Q)|_{\omega=\bar{\omega}_{ij}}$  to the initial condition in the interval  $(m_{ij}, M_{ij})$  of  $m_Q$ . The insensitivity to the variable  $\omega$  commands the vanishing of the first derivative in Eq. (7),  $d\Delta\rho_{ij}(m_Q)/d\omega|_{\omega=\bar{\omega}_{ij}} = 0$ , from which roots of  $m_Q$  are solved. Furthermore, the second derivative  $d^2\Delta\rho_{ij}(m_Q)/d\omega^2|_{\omega=\bar{\omega}_{ij}}$  should be minimal to maximize the stability window around  $\bar{\omega}_{ij}$ , in which  $\Delta\rho_{ij}(m_Q)$  remains almost independent of  $\omega$ .

The threshold behaviors in Eq. (3) and the initial conditions  $\Delta\rho_{ij}(m_Q) = -\text{Im}\Pi_{ij}^{\text{box}}(m_Q)$  with  $\text{Im}\Pi_{ij}^{\text{box}}(m_Q)$  being defined according to Eq. (4) set the initial conditions in the limits  $m_Q \rightarrow m_{ij}$ ,

$$\begin{aligned} \Delta\rho_{db}(m_Q) &\sim m_Q^2 - m_b^2, \\ \Delta\rho_{sb}(m_Q) &\sim [m_Q^2 - (m_b + m_s)^2]^{-1/2}, \\ \Delta\rho_{bb}(m_Q) &\sim (m_Q^2 - 4m_b^2)^{1/2}. \end{aligned} \quad (8)$$

The solution in Eq. (6) scales in the threshold region  $m_Q \sim m_{ij}$  like  $\Delta\rho_{ij}(m_Q) \sim [m_Q^2 - (m_i + m_j)^2]^{\alpha_{ij}}$  owing to the relation  $J_\alpha(z) \sim z^\alpha$  in the limit  $z \rightarrow 0$ . Contrasting this scaling law with Eq. (8), we read off the indices

$$\alpha_{db} = 1, \quad \alpha_{sb} = -1/2, \quad \alpha_{bb} = 1/2. \quad (9)$$

It is clear now why we employed those modified integrands in Eq. (4); the corresponding inputs in Eq. (8) are proportional to simple powers of  $m_Q^2 - (m_i + m_j)^2$ , so that the indices  $\alpha_{ij}$  can be specified unambiguously. The coefficients  $y_{ij}$  are related to the boundary conditions at the high end  $m_Q = M_{ij}$  of the interval  $(m_{ij}, M_{ij})$ ,  $\Delta\rho_{ij}(M_{ij}) = -\text{Im}\Pi_{ij}^{\text{box}}(M_{ij})$ , which fix the coefficients

$$y_{ij} = -\text{Im}\Pi_{ij}^{\text{box}}(M_{ij}) \left[ \left( \omega \sqrt{M_{ij}^2 - (m_i + m_j)^2} \right)^{\alpha_{ij}} \times J_{\alpha_{ij}} \left( 2\omega \sqrt{M_{ij}^2 - (m_i + m_j)^2} \right) \right]^{-1}. \quad (10)$$

The running coupling constant is given by

$$\alpha_s(\mu) = \frac{4\pi}{\beta_0 \ln(\mu^2/\Lambda_{\text{QCD}}^2)} \left[ 1 - \frac{\beta_1 \ln \ln(\mu^2/\Lambda_{\text{QCD}}^2)}{\beta_0^2 \ln(\mu^2/\Lambda_{\text{QCD}}^2)} \right], \quad (11)$$

with the coefficients  $\beta_0 = 11 - 2n_f/3$  and  $\beta_1 = 2(51 - 19n_f/3)$ . We take the QCD scale  $\Lambda_{\text{QCD}} = 0.21$  GeV for the number of active quark flavors  $n_f = 5$  [26] and choose the renormalization scale  $\mu = m_Q$  as stated before. Note that we need only the quark-mass inputs for the initial conditions in the interval  $(m_{ij}, M_{ij})$  of  $m_Q$ . Adopting the quark masses  $m_s = 0.1$  and  $m_b = 4.15$  GeV in the  $\overline{\text{MS}}$  scheme at the scale  $\mu \sim m_b$ , which are close to those from lattice calculations [27], and the pion (kaon,  $B$ -meson) mass  $m_\pi = 0.14$  GeV ( $m_K = 0.49$ ,  $m_B = 5.28$  GeV) [28], we get  $\bar{\omega}_{db} = 0.0531$ ,  $\bar{\omega}_{sb} = 0.0268$ ,  $\bar{\omega}_{bb} = 0.0128$  GeV $^{-1}$  from the best fits of  $\Delta\rho_{ij}(m_Q)$  in Eq. (6) to  $-\text{Im}\Pi_{ij}^{\text{box}}(m_Q)$  in the interval  $(m_{ij}, M_{ij})$ . The fit results by means of  $\Delta\Gamma_{ij}(m_Q)$ , which are related to  $\Delta\rho_{ij}(m_Q)$  via Eq. (4), are compared with

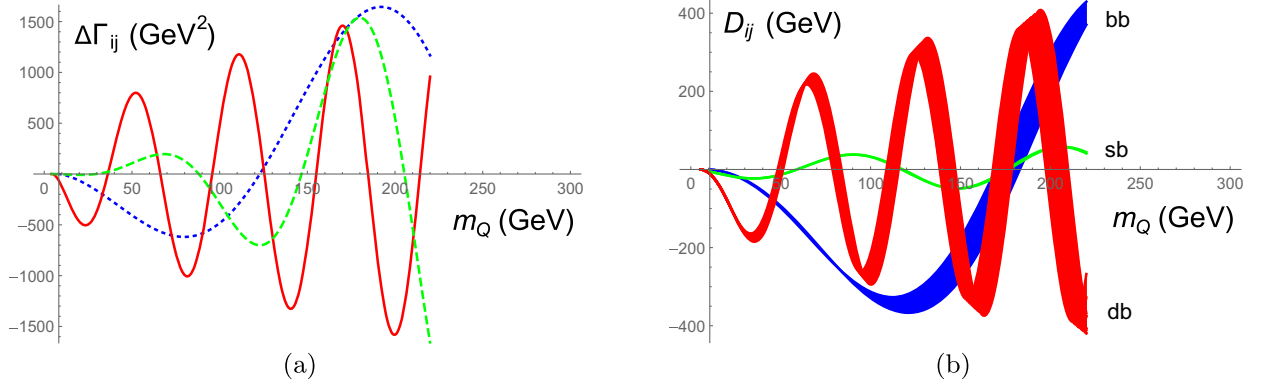


FIG. 3. (a) Dependencies of the solutions  $\Delta\Gamma_{ij}(m_Q)$  on  $m_Q$  for  $ij = db$  (solid line),  $ij = sb$  (scaled by a factor 0.02, dashed line), and  $ij = bb$  (scaled by a factor 0.1, dotted line). (b) Dependencies of the derivatives  $D_{ij}(m_Q)$  on  $m_Q$ .

$-\Gamma_{ij}^{\text{box}}(m_Q)$  in the interval  $(m_{ij}, M_{ij})$  in Fig. 2. Their perfect matches confirm that the approximate solutions in Eq. (6) work well and that other methods for obtaining  $\bar{\omega}_{ij}$  should return similar values. For example, equating  $\Delta\rho_{ij}(m_Q)$  and  $-\text{Im}\Pi_{ij}^{\text{box}}(m_Q)$  at the midpoints  $m_Q = (m_{ij} + M_{ij})/2$  leads to  $\bar{\omega}_{db} = 0.0503$ ,  $\bar{\omega}_{sb} = 0.0268$ , and  $\bar{\omega}_{bb} = 0.0129$  GeV<sup>-1</sup>, very close to those from the best fits.

The unknown subtracted functions  $\Delta\rho_{ij}(m_Q)$  with the above  $\alpha_{ij}$ ,  $y_{ij}$ , and  $\bar{\omega}_{ij}$  are displayed in Fig. 3(a) through  $\Delta\Gamma_{ij}(m_Q)$ . They exhibit oscillatory behaviors in  $m_Q$ , and the first (second, third) peak of the solution for the  $bb$  ( $sb$ ,  $db$ ) channel is located around  $m_Q \approx 170-195$  GeV. The coincidence between the sequences of the peaks and of the quark generations is intriguing. The similar feature will appear again in the plots for the fourth generation quark masses in the next section. To evince the implication of the above peak overlap, we present in Fig. 3(b) the dependencies of the derivatives  $d\Delta\rho_{ij}(m_Q)/d\omega$  on  $m_Q$  by

$$D_{ij}(m_Q) \equiv \frac{d}{d\omega} \frac{J_{\alpha_{ij}}(2\omega\sqrt{m_Q^2 - (m_i + m_j)^2})}{J_{\alpha_{ij}}(2\omega\sqrt{M_{ij}^2 - (m_i + m_j)^2})} \Big|_{\omega=\bar{\omega}_{ij}}, \quad (12)$$

where the factors independent of  $\omega$  have been dropped for simplicity.

The band of the  $bb$  curve is induced by the variation of the bottom-quark mass  $m_b$  in the range  $m_b = (4.15 \pm 0.01)$  GeV with roughly  $1\sigma$  deviation from the value  $4.18_{-0.02}^{+0.03}$  GeV in [28]. The considered error of  $m_b$  is also compatible with that obtained in Ref. [27]. The result for the  $db$  channel is less sensitive to  $m_b$ , but depends more strongly on the methods of determining  $\bar{\omega}_{db}$  as mentioned before. Namely, the band of the  $db$  curve is mainly attributed to the latter source of uncertainties with  $\bar{\omega}_{db}$  being lowered to  $0.0503$  GeV<sup>-1</sup>. The derivative  $D_{sb}(m_Q)$  is stable with respect to various sources of uncertainties; for instance, changing the strange-quark mass  $m_s$  by 10%

causes only about 1% effects. It is the reason why the  $sb$  curve discloses a narrow band. Every curve in Fig. 3(b) indicates the existence of multiple roots. It has been checked that the second derivatives are larger at higher roots [1], so smaller roots are preferred in the viewpoint of maximizing the stability windows in  $\omega$ . Figure 3(b) shows that the three derivatives first vanish simultaneously around  $m_Q \approx 173$  GeV, as manifested by the intersection of the three curves in the interval (170, 176 GeV), which corresponds to the location of the peak overlap in Fig. 3(a). To be explicit, we read off the roots  $m_Q = 169.1_{-1.1}^{+9.5}$  GeV for the  $db$  channel,  $m_Q = 176.2 \pm 0.6$  GeV for the  $sb$  channel, and  $m_Q = 175.7_{-6.3}^{+7.3}$  GeV for the  $bb$  channel in Fig. 3(b). The result of  $m_Q$ , as a common solution to the considered channels, is identified as the physical top-quark mass, which agrees well with the observed one  $m_t = (172.69 \pm 0.30)$  GeV [28].

A remark is in order. The tiny error 0.01 GeV for the input  $m_b = (4.15 \pm 0.01)$  GeV was adopted to examine the sensitivity of our predictions to the variation of the bottom-quark mass. We emphasize that the main purpose of the present work is to predict the fourth generation quark masses, for which both the bottom- and top-quark masses are necessary inputs. Hence, the reproduction of the top-quark mass from the given bottom-quark mass in its allowed range is not only to validate our formalism, but to calibrate the inputs for the predictions. This calibration is essential owing to the sensitivity to the inputs as noticed above (the determination of the lighter quark masses in our formalism is more stable against variations of inputs [1]). Additionally, we set the renormalization scale to the invariant mass  $m_Q$  of the heavy quark in Eq. (2) and stick to this choice for the consistent determination of the top-quark mass and the fourth generation quark masses. We think that  $m_b = 4.15 \pm 0.01$  GeV and the resultant  $m_t = 173 \pm 3$  GeV, in agreement with the extractions from other known means and current data, serve as the appropriate inputs. Note that only the outcome from the  $bb$  channel, which involves two bottom quarks in the

intermediate states, is sensitive to the input of  $m_b$ . Therefore, a resolution to the aforementioned sensitivity that one can make is to discard the  $bb$  channel and to consider simply the  $db$  and  $sb$  channels. The simultaneous vanishing of their derivatives in Eq. (12) is sufficient for deriving a stable and definite top-quark mass.

### III. FOURTH GENERATION QUARK MASSES

After verifying that the dispersive analysis produces the correct top-quark mass, we extend it to the predictions of the fourth generation quark masses, starting with the  $b'$  one. Consider the box diagrams for the mixing of the neutral states  $Q\bar{d}$  and  $\bar{Q}d$  and construct the associated dispersion relations. The intermediate channels, which contribute to the imaginary pieces of the box diagrams, contain not only those from on-shell quarks  $ut$ ,  $ct$ , and  $tt$  described by Eq. (2), but those from on-shell  $W$  bosons. Since these channels can be differentiated experimentally, we can focus on the former for our purpose. The necessary power corrections proportional to the differences between the quark-level thresholds  $m_{ij}$  and the physical thresholds  $M_{ij}$  further select the  $ut$  channel with  $m_{ut} = m_t$  ( $m_u = 0$ ) and

$M_{ut} = m_\pi + m_t$ , and the  $ct$  channel with  $m_{ct} = m_c + m_t$  and  $M_{ct} = m_D + m_t$ , with  $m_D$  being the  $D$ -meson mass. Note that the second term in the curly brackets of Eq. (2) becomes more important in the present case owing to the large ratio  $(m_i^2 + m_j^2)/m_W^2 \approx m_i^2/m_W^2$ . Equation (2) behaves approximately in the threshold regions with  $m_Q \sim m_{ij}$  like

$$\begin{aligned}\Gamma_{ut}^{\text{box}}(m_Q) &\sim \frac{(m_Q^2 - m_t^2)^2}{m_Q^2}, \\ \Gamma_{ct}^{\text{box}}(m_Q) &\sim \frac{m_Q^2 - m_t^2 - m_c^2}{m_Q^2} \\ &\quad \times \sqrt{[m_Q^2 - (m_t + m_c)^2][m_Q^2 - (m_t - m_c)^2]}.\end{aligned}\quad (13)$$

Because of  $m_c \ll m_t$ , the terms  $(m_t - m_c)^2$  and  $m_t^2 + m_c^2$ , which are not very distinct from  $(m_t + m_c)^2$ , have stayed in the second expression of Eq. (13).

Motivated by the above threshold behaviors, we choose the integrands for the dispersion integrals in Eq. (1) as

$$\begin{aligned}\text{Im}\Pi_{ut}(m) &= \frac{m^2\Gamma_{ut}(m)}{m^2 - m_t^2}, \\ \text{Im}\Pi_{ct}(m) &= \frac{m^2\Gamma_{ct}(m)}{[m^2 - (m_t + m_c)^2](m_Q^2 - m_t^2 - m_c^2)\sqrt{m^2 - (m_t - m_c)^2}}.\end{aligned}\quad (14)$$

Similarly, the above integrands with powers of  $m$  in the numerators suppress the residues from the poles at  $m = \pm(m_i + m_j)$  and  $m = \pm\sqrt{m_i^2 + m_j^2}$  in the low- $m$  region, compared to the ones from  $m = \pm m_Q$  at large  $m_Q$ . Our contour for  $\Pi_{ct}(m)$  crosses the real axis between  $m = -(m_t + m_c)$  and  $m = -\sqrt{m_t^2 + m_c^2}$  and between  $m = \sqrt{m_t^2 + m_c^2}$  and  $m = m_t + m_c$  and runs along the real axis marked by  $m < -(m_t + m_c)$  and  $m > m_t + m_c$ . Therefore, the branch cut associated with the factor  $\sqrt{m^2 - (m_t - m_c)^2}$  in  $\Pi_{ct}(m)$  does not contribute. The solutions for the unknown subtracted functions  $\Delta\rho_{ij}(m_Q)$  and the coefficients  $y_{ij}$  have the same forms as Eqs. (6) and (10), respectively. The initial conditions near the thresholds  $m_Q \sim m_{ij}$  are given by

$$\begin{aligned}\Delta\rho_{ut}(m_Q) &\sim m_Q^2 - m_t^2, \\ \Delta\rho_{ct}(m_Q) &\sim [m_Q^2 - (m_t + m_c)^2]^{-1/2},\end{aligned}\quad (15)$$

which assign the indices

$$\alpha_{ut} = 1, \quad \alpha_{ct} = -1/2.\quad (16)$$

For the numerical study, we take the QCD scale  $\Lambda_{\text{QCD}}^{(6)} = 0.11$  GeV for the number of active quark flavors  $n_f = 6$  according to [29]

$$\Lambda_{\text{QCD}}^{(n_f)} = \Lambda_{\text{QCD}}^{(n_f-1)} \left[ \frac{\Lambda_{\text{QCD}}^{(n_f-1)}}{m_t} \right]^{2/(3\beta_0)},\quad (17)$$

with  $m_t = 173$  and  $\Lambda_{\text{QCD}}^{(5)} = 0.21$  GeV [26]. The behaviors of the box-diagram contributions  $\Gamma_{ij}^{\text{box}}(m_Q)$  in the interval  $(m_{ij}, M_{ij})$  of  $m_Q$  matter in solving the dispersion relations. In view of the high top-quark mass, the renormalization-group (RG) evolution of the charm-quark mass to a scale of  $O(m_t)$  needs to be taken into account. This RG effect is minor in the previous section, since  $m_b$  does not deviate much from the range  $\mu \approx 1\text{--}2$  GeV, in which the strange-quark mass is defined. We have at  $\mu = m_t$  [26]

$$m_c(m_t) = m_c(m_c) \left[ \frac{\alpha_s(m_t)}{\alpha_s(m_c)} \right]^{4/\beta_0} \approx 0.7 \text{ GeV},\quad (18)$$

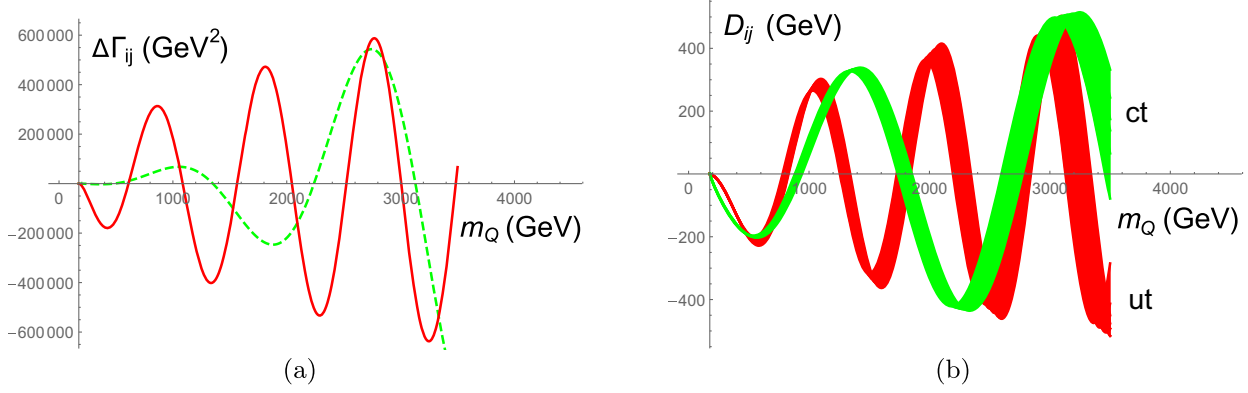


FIG. 4. (a) Dependencies of the solutions  $\Delta\Gamma_{ij}(m_Q)$  on  $m_Q$  for  $ij = ut$  (solid line) and  $ij = ct$  (scaled by a factor 0.02, dashed line). (b) Dependencies of the derivatives  $D_{ij}(m_Q)$  on  $m_Q$ . The curve for  $ij = ut$  has been scaled by a factor 0.01.

for  $m_c(m_c) = 1.35$  GeV [1]. The inputs of the pion mass  $m_\pi = 0.14$  GeV and the  $D$ -meson mass  $m_D = 1.87$  GeV [28] then yield  $\bar{\omega}_{ut} = 0.00326$  and  $\bar{\omega}_{ct} = 0.00176$  GeV $^{-1}$  from the best fits of Eq. (6) to  $-\text{Im}\Pi_{ij}^{\text{box}}(m_Q)$  in the interval  $(m_{ij}, M_{ij})$  of  $m_Q$ , which is proportional to Eq. (2). Equating  $\Delta\rho_{ij}(m_Q)$  and  $-\Pi_{ij}^{\text{box}}(m_Q)$  at the mid-points  $m_Q = (m_{ij} + M_{ij})/2$  generates  $\bar{\omega}_{ut} = 0.00326$  and  $\bar{\omega}_{ct} = 0.00175$  GeV $^{-1}$ , almost identical to the values from the best fits. This consistency supports the goodness of our solutions.

The dependencies of the unknown subtracted functions  $\Delta\rho_{ij}(m_Q)$  on  $m_Q$  from solving the dispersion relations are presented in Fig. 4(a) by means of  $\Delta\Gamma_{ij}(m_Q)$ . We have confirmed the excellent matches between  $\Delta\Gamma_{ij}(m_Q)$  from the fits and the initial conditions  $-\Gamma_{ij}^{\text{box}}(m_Q)$  in the interval  $(m_{ij}, M_{ij})$  of  $m_Q$ , which will not be shown here. The feature noticed before hints that the second (third) peak of the curve for the  $ct$  ( $ut$ ) channel should be located at roughly the same  $m_Q$ . Figure 4(a), with the overlap of peaks around  $m_Q \approx 2.7$  TeV, corroborates this expectation. The corresponding derivatives in Eq. (12) as functions of  $m_Q$  are drawn in Fig. 4(b). Similarly, our results for the  $ct$  channel are insensitive to the variation of  $m_c$ : 10% changes of  $m_c$  stimulates only about 1% effects on the outcome of the fourth generation quark mass  $m_{b'}$ . The uncertainties from different ways of fixing  $\bar{\omega}_{ij}$  are negligible as investigated above. Hence, we consider only the uncertainties from the variation of the top-quark mass within  $m_t = (173 \pm 3)$  GeV attained in the previous section, which are reflected by the bands of the curves. It is found that the two derivatives first vanish simultaneously around  $m_Q \approx 2.7$  TeV, coinciding with the location of the peak overlap in Fig. 4(a). That is, a common solution  $m_{b'} = (2.7 \pm 0.1)$  TeV, as inferred from Fig. 4(b), exists for the two considered channels.

The prediction of the fourth generation quark mass  $m_{t'}$  proceeds in exactly the same manner. The box diagrams governing the mixing of the neutral states  $Q\bar{u}$  and  $Q\bar{u}$

involve the intermediate  $db'$ ,  $sb'$ , and  $bb'$  channels, which are associated with the quark-level thresholds  $m_{db'} = m_{b'}$  ( $m_d = 0$ ),  $m_{sb'} = m_s + m_{b'}$ , and  $m_{bb'} = m_b + m_{b'}$  and the physical thresholds  $M_{db'} = m_\pi + m_{b'}$ ,  $M_{sb'} = m_K + m_{b'}$ , and  $M_{bb'} = m_B + m_{b'}$ , respectively. Since a top quark does not form a hadronic bound state, we do not expect that a  $b'$  quark will, and so we keep the quark mass  $m_{b'}$  in the hadronic thresholds. Certainly, this is an assumption owing to the uncertain  $4 \times 4$  CKM matrix element  $V_{tb'}$ . The second term in the curly brackets of Eq. (2) dominates because of the large ratio  $(m_i^2 + m_j^2)/m_W^2 \approx m_{b'}^2/m_W^2$ . The behaviors of Eq. (2) in the threshold regions with  $m_Q \sim m_{ij}$  are approximated by Eq. (13), with the first expression for the  $db'$  channel and the second expression for the  $sb'$  and  $bb'$  channels. The appropriate replacements of the masses  $m_{c,t}$  by  $m_{s,b,b'}$  are understood. The modified integrands for the dispersion integrals in Eq. (1) and their expressions near the thresholds  $m_Q \sim m_{ij}$  follow Eqs. (14) and (15), respectively, also with the first lines for the  $db'$  channel and the second lines for the  $sb'$  and  $bb'$  channels. We then acquire the indices

$$\alpha_{db'} = 1, \quad \alpha_{sb'} = \alpha_{bb'} = -1/2. \quad (19)$$

The QCD scale takes the value  $\Lambda_{\text{QCD}}^{(7)} = 0.04$  GeV for  $n_f = 7$  according to Eq. (17), but with  $m_{b'}$  being substituted for  $m_t$ . The RG effects on the quark masses are included via Eq. (18), which give  $m_s \approx 0.07$  and  $m_b \approx 3.2$  GeV at the scale  $\mu = m_{b'}$ . Inputting the same masses  $m_\pi$ ,  $m_K$ ,  $m_B$ , and  $m_{b'} = 2.7$  TeV, we get  $\bar{\omega}_{db'} = 0.0438$ ,  $\bar{\omega}_{sb'} = 0.0223$ , and  $\bar{\omega}_{bb'} = 0.0233$  TeV $^{-1}$  from the best fits of Eq. (6) to  $-\text{Im}\Pi_{ij}^{\text{box}}(m_Q)$  in the interval  $(m_{ij}, M_{ij})$  of  $m_Q$ . Figure 5(a) collects the solutions  $\Delta\Gamma_{ij}(m_Q)$  as functions of  $m_Q$ , where the curves for the  $bb'$  and  $sb'$  channels are close in shape, and their second peaks overlap with the third peak for the  $db'$  channel around  $m_Q \approx 200$  TeV. The  $bb'$  and  $sb'$  channels share the identical formula characterized by the same indices  $\alpha_{sb'} = \alpha_{bb'} = -1/2$ . Moreover, the difference

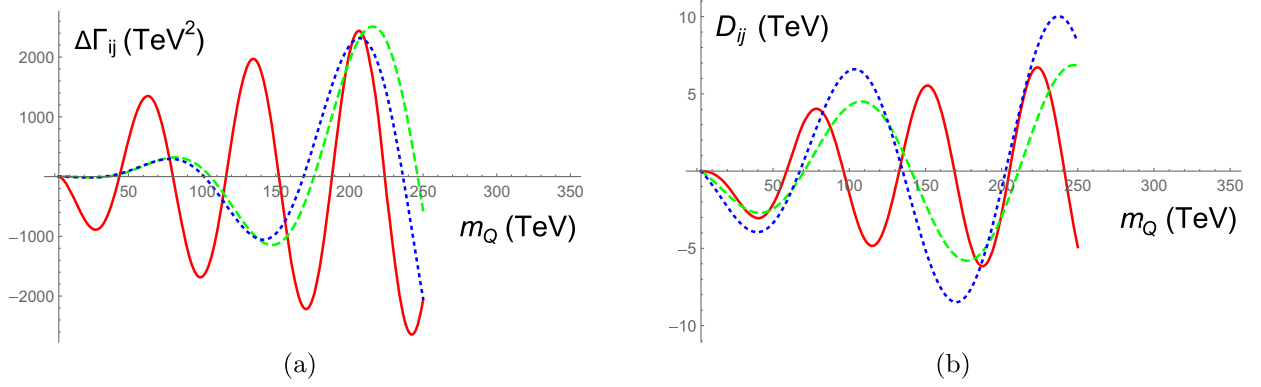


FIG. 5. (a) Dependencies of the solutions  $\Delta\Gamma_{ij}(m_Q)$  on  $m_Q$  for  $ij = db'$  (solid line),  $ij = sb'$  (scaled by a factor 0.02, dashed line), and  $ij = bb'$  (scaled by a factor 0.02, dotted line). (b) Dependencies of the derivatives  $D_{ij}(m_Q)$  on  $m_Q$  for  $ij = db'$  (scaled by a factor  $10^{-4}$ , solid line),  $ij = sb'$  (dashed line), and  $ij = bb'$  (dotted line).

between  $m_s$  and  $m_b$  (also between  $m_K$  and  $m_B$ ) is minor relative to the high  $m_{b'}$ , so that these two solutions behave similarly. Hence, there are only two categories of solutions in the  $t'$  case, and the overlap takes place between the second and third peaks.

The dependencies of the derivatives  $D_{ij}(m_Q)$  on  $m_Q$ , defined in Eq. (12), are displayed in Fig. 5(b) for  $\omega = \bar{\omega}_{ij}$ . The three derivatives first vanish simultaneously around  $m_Q \approx 200$  TeV, which coincides with the aforementioned peak locations. It is sure that a common root for the fourth generation quark mass  $m_{t'}$  exists. Since the value of  $m_{t'}$  is obviously beyond the current and future reach of new particle searches, we do not bother to include theoretical uncertainties with the prediction. One may wonder whether  $m_{t'} \approx 200$  TeV violates the unitarity limit signified by the large Yukawa coupling. However, bound states would be formed in this case, such that physical degrees of freedom change, and the high Yukawa coupling is not an issue. This subject will be elaborated in the next section. It is not unexpected that a  $t'$  quark is so heavy, viewing that a  $c$  quark is 13 times heavier than an  $s$  quark, and a  $t$  quark is about 40 times heavier than a  $b$  quark. Here a  $t'$  quark is about 70 times heavier than a  $b'$  quark.

#### IV. $\bar{b}'b'$ BOUND STATES

As remarked in the Introduction, the sequential fourth generation model is disfavored by the data of Higgs boson production via gluon fusion and decay into photon pairs [14]. Nevertheless, it has been known [16] that the fourth generation quarks, whose mass  $m_Q$  meets the criterion  $K_Q = m_Q^3 / (4\pi v^2 m_H) > 1.68$ , with the vacuum expectation value  $v = 246$  GeV, form bound states in a Yukawa potential. The binding energy for the  $\bar{Q}Q$  ground state with the masses  $m_Q^* \approx 1.26$  and  $m_H^* \approx 1.45$  TeV at the fixed point of the RG evolution in this model was found to be  $-4.9$  GeV. The fixed point depends on the initial values of the quark masses at the electroweak scale of  $O(100)$  GeV: the larger the initial values, the lower the fixed point is.

The  $b'$ -quark mass  $m_{b'} = 2.7$  TeV predicted in the previous section, greater than the fixed-point value 1.26 TeV, satisfies the criterion  $K_Q > 1.68$  definitely. The binding energy for the  $\bar{b}'b'$  bound state ought to be higher. We will demonstrate that the new scalars  $S$  formed by  $\bar{b}'b'$ , with tiny couplings to a Higgs boson, escape the current experimental constraints. It is then worthwhile to keep searching for a superheavy  $b'$  quark at future colliders [30].

Once the bound state of mass at TeV scale is formed, the gluon fusion process involving internal  $b'$  quarks at the low scale  $m_H$  should be analyzed in an effective theory with different physical degrees of freedom. In other words, one has to regard the process as gluon fusion into the scalar  $S$ , followed by production of a Higgs boson through a coupling between them. The order of magnitude of the corresponding amplitude is assessed below. First, the gluon fusion into  $S$  is proportional to  $\sqrt{s}g_{ggS}$ , where the invariant mass  $\sqrt{s}$  of  $S$  takes into account the dimension of the effective operator  $A^\mu A^\nu S$ , with  $A^\mu$  being a gluon field, and where  $g_{ggS}$  is a dimensionless effective coupling. The scalar  $S$  then propagates according to a Breit-Wigner factor  $1/(s - m_S^2 - i\sqrt{s}\Gamma_S)$ , where  $\Gamma_S$  denotes the width of  $S$ . At last,  $S$  transforms into a Higgs boson  $H$  with the magnitude being described by  $sg_{SH}$ , where  $g_{SH}$  is a dimensionless effective coupling. The total amplitude is thus written, in the effective approach, as

$$\mathcal{M} \sim \frac{\sqrt{s}^3 g_{ggS} g_{SH}}{s - m_S^2 - i\sqrt{s}\Gamma_S}, \quad (20)$$

where factors irrelevant to our reasoning have been suppressed.

Properties of heavy quarkonium states, like  $\bar{b}'b'$ , in a Yukawa potential

$$V(r) = -\alpha_Y \frac{e^{-m_H^* r}}{r}, \quad (21)$$



of the strength  $\alpha_Y = m_{b'}^2/(4\pi v^2)$ , have been explored extensively in the literature (for a recent reference, see Ref. [31]). With the involved superheavy quark-mass scale, we have adopted the fixed-point Higgs boson mass  $m_H^*$  in the exponential. Note that the number of bound states is finite for a Yukawa potential, distinct from the case for a Coulomb potential which allows infinitely many bound-state solutions. It turns out that only the states characterized by  $(n, l) = (1, 0), (2, 0), (2, 1), (3, 0),$  and  $(3, 1)$  are bounded,  $n$  ( $l$ ) being the principal (angular momentum) quantum number. The states labeled by  $(n, l) = (3, 2)$  or higher quantum numbers are not bounded. The ground state with  $(n, l) = (1, 0)$ , being either a pseudoscalar or a vector, is expected to have a negligible coupling to a Higgs boson. It is easy to read off the value  $\epsilon_{10} = -0.75$  of this state from Fig. 1 in [31], i.e., the binding energy  $E_{10} \equiv \alpha_Y^2 m_{b'} \epsilon_{10}/4 \approx -41$  TeV, for the parameter  $1/(m_H^* a_0) = 8.9$ , with  $a_0 \equiv 2/(\alpha_Y m_{b'})$  being the Bohr radius. It is apparent that this deep ground state has revealed the nonrelativistic Thomas collapse [32] and calls for a relativistic treatment [17,33].

To examine the coupling to a Higgs boson, we concentrate on the  $P$ -wave scalar states with  $l = 1$ , and deduce the value  $\epsilon_{21} = -0.08$  for the  $(n, l) = (2, 1)$  state from Fig. 2 in [31], i.e., the binding energy  $E_{21} \equiv \alpha_Y^2 m_{b'} \epsilon_{21}/4 \approx -4.96$  TeV. We suspect that this deep bound state also suffers from the Thomas collapse, but continue our order-of-magnitude estimate for completeness. Figure 5 in [31] provides the first derivative of the corresponding wave function at the origin

$$32\pi a_0^5 |\psi'_{21}(0)|^2 \approx 0.7, \quad (22)$$

for the parameter  $\delta = m_H^* a_0 = 0.11$ . The width  $\Gamma_S$  is then approximated by the  $S \rightarrow gg$  decay width as in the heavy quarkonium case [34],

$$\Gamma_S = 48\alpha_S^2 (2m_{b'}) \frac{|R'_{21}(0)|}{m_S} \approx 570 \text{ GeV}, \quad (23)$$

where the strong coupling has been evaluated at twice the  $b'$ -quark mass,  $R'_{nl}(0) = \sqrt{4\pi/3} \psi'_{nl}(0)$  is the derivative of the radial wave function at the origin [31], and the scalar has the mass  $m_S = 2m_{b'} + E_{21} \approx 440$  GeV. The width in Eq. (23) is larger than the scalar mass, signaling another warning to the consistency of this state.

To pin down the product of the effective couplings  $g_{ggS}g_{SH}$ , we match the amplitude in Eq. (20) to the one in the fundamental theory by considering the production of a fictitious Higgs boson with mass squared  $s \approx m_S^2$ . The involved scale is so high that the evaluation in the fundamental theory [35,36] based on the direct annihilation of the  $\bar{b}'b'$ -quark pair ought to yield a result the same as in the effective approach. We identify the part of the amplitude, which approaches  $3/2$  in the lowest-order expression from the fundamental theory [35,36],

$$\left| \frac{v}{s} \frac{\sqrt{s^3} g_{ggS} g_{SH}}{s - m_S^2 - i\sqrt{s}\Gamma_S} \right|^2 \approx \left( \frac{v g_{ggS} g_{SH}}{\Gamma_S} \right)^2 \approx \left( \frac{3}{2} \right)^2. \quad (24)$$

The factor  $s - m_S^2 \ll \sqrt{s}\Gamma_S$  has been ignored in the denominator for  $s \approx m_S^2$  on the right-hand side of the first equal sign. Equation (24) implies  $g_{ggS}g_{SH} = (2/3)\Gamma_S/v$  obviously. We then obtain, by extrapolating Eq. (20) to  $s = m_H^2$ , the suppression factor on the  $S$  contribution relative to the top-quark one in the SM,

$$\left| \frac{v}{s} \frac{\sqrt{s^3} g_{ggS} g_{SH}}{s - m_S^2 - i\sqrt{s}\Gamma_S} \right|^2 \approx \left( \frac{2 m_H \Gamma_S}{3 m_S^2} \right)^2 \approx 6.2\%. \quad (25)$$

The above result also suggests that the  $S$  contribution decreases like  $m_S^{-4}$ .

We repeat the discussion for the  $(n, l) = (3, 1)$  state, whose binding energy and the first derivative of the corresponding wave function at the origin read

$$E_{31} \equiv \frac{1}{4} \alpha_Y^2 m_{b'} \epsilon_{31} \approx -124 \text{ GeV},$$

$$\frac{729}{8} \pi a_0^5 |\psi'_{31}(0)|^2 \approx 0.2, \quad (26)$$

with  $\epsilon_{31} = -0.002$  according to Figs. 2 and 5 in [31], respectively. The width  $\Gamma_S$  in Eq. (23) is given, for this state, by

$$\Gamma_S = 48\alpha_S^2 (2m_{b'}) \frac{|R'_{31}(0)|}{m_S} \approx 694 \text{ GeV}, \quad (27)$$

with  $m_S = 2m_{b'} + E_{31} \approx 5.28$  TeV. The similar matching procedure leads to the diminishing suppression factor

$$\left( \frac{2 m_H \Gamma_S}{3 m_S^2} \right)^2 \approx 4.3 \times 10^{-6}, \quad (28)$$

on the  $S$  contribution to the Higgs boson production via gluon fusion in the SM.

We confront the above estimates with those from the relativistic calculation [33], whose Eq. (28) indeed allows only the bound-state solutions characterized by  $n = 1, 2,$  and  $3$ . Because of their crude approximation, the states labeled by the same  $n$  but different  $l$  are degenerate in eigenenergies. We take the positive eigenenergy  $E_n$  from Eq. (28) of [33], extract the binding energy  $E_n^b = E_n - m_{b'}/2$  with  $m_{b'}/2$  being the reduced mass of the  $\bar{b}'b'$  system, and derive the bound-state mass  $m_S = 2m_{b'} + E_n^b$ . It is trivial to get the ground-state mass 3.23 TeV, the mass of the first excited state 4.45 TeV for  $n = 2$ , and the mass of the second excited state  $\lesssim 5.40$  TeV for  $n = 3$ . The last value, differing from the nonrelativistic one 5.28 TeV by only 2%, confirms that this state is loosely bound. The masses of the first two states from the relativistic

framework look more reasonable. We mention that a recent study of the oblique parameters  $S$  and  $T$  has permitted heavy resonances to be heavier than 3 TeV [37]. Equations (23) and (27) hint that the widths of these bound states are of the same order of magnitude, so Eq. (25) indicates a tiny contribution from the  $n = 2$  state at  $10^{-3}$  level to the Higgs boson production via gluon fusion. We conclude that the  $S$  contributions are negligible compared with the SM one. It is thus likely that a fourth generation quark as heavy as 2.7 TeV bypasses the constraint of the measured  $gg \rightarrow H$  cross section at the scale  $s \sim m_H^2$ .

The same observation holds for the constraint on the fourth generation quarks from the data of the Higgs decay into photon pairs. The reasoning related to the  $H \rightarrow \gamma\gamma$  decay proceeds in a similar way. One just replaces the effective coupling  $g_{ggS}$  in Eq. (24) by  $g_{\gamma\gamma S}$  and the constant  $3/2$  on the right-hand side of Eq. (24) by  $1/2$ , which takes into account the color factor for the quark loop and the electric charge of a top quark. We then estimate the suppression factor on the  $S$  contribution relative to the top-quark one,

$$\left(2 \frac{m_H \Gamma_S}{m_S^2}\right)^2 \approx 10^{-2}. \quad (29)$$

That is, the contribution from the  $\bar{b}'b'$  bound state to the  $H \rightarrow \gamma\gamma$  decay is also negligible.

It is impossible to detect a  $t'$  quark with a mass as high as 200 TeV in the foreseeable future. To detect a  $b'$  quark, the gluon fusion into a  $\bar{b}'b'$  resonance of mass about 3.2 TeV may not be efficient owing to the small gluon distribution functions at large parton momenta. Instead, the fusion process  $qq \rightarrow WW, ZZ \rightarrow S$  [38] is more promising, whose cross section is enhanced by the quark distribution functions. Another promising channel is the  $W$ -boson mediated single  $b'$ -quark production associated with a top quark and a light quark, such as  $dq \rightarrow u\bar{t}b'$ . It gains the power enhancement with one fewer virtual weak boson by paying the price of having a smaller gluon distribution function. Presuming that  $b'$  decays into  $tW$  dominantly, one can search for an excess of  $t\bar{t}W$  final states [39,40]. The analysis is analogous to the search of vectorlike heavy quarks [41], and the currently available strategies work. Another simpler single  $b'$ -quark production from the  $ug \rightarrow W^+b'$  process may be attempted, which, however, suffers the uncertain suppression of the diminishing  $4 \times 4$  CKM matrix element  $V_{ub'}$ .

## V. CONCLUSION

After accumulating sufficient clues in our previous studies that the scalar sector of the SM can be stringently constrained and there might be only three fundamental parameters from the gauge groups, we delved into the sequential fourth generation model as a natural extension of

the SM. It has been demonstrated that the fourth generation quark masses can be predicted in the dispersive analyses of neutral quark state mixing involving a heavy quark. The idea is to treat the dispersion relations obeyed by the mixing observables as inverse problems with the initial conditions from the box-diagram contributions in the interval between the quark-level and hadronic thresholds. A heavy quark must take a specific mass in order to ensure a physical solution for the mixing observable to be invariant under the arbitrary scaling of the heavy-quark mass in the dispersive integrals. We first worked on the mixing mediated by the  $db$ ,  $sb$ , and  $bb$  channels and showed that the roots of the heavy-quark mass  $m_Q$  corresponding to the first (second, third) peaks of the  $bb$  ( $sb$ ,  $db$ ) contributions, with the inputs of the typical strange- and bottom-quark masses, coincide around  $m_Q \approx 173$  GeV. This outcome, highly nontrivial from the three independent channels and in agreement with the measured top-quark mass, affirms our claim that the scalar interaction introduced to couple different generations in the SM is not discretionary.

Encouraged by the successful explanation of the top-quark mass, we applied the formalism to the predictions for the fourth generation quark masses. The perturbative inputs to the dispersion relations come from the same box diagrams involving multiple intermediate channels, i.e., the  $ut$  and  $ct$  channels in the  $b'$  case and the  $db'$ ,  $sb'$ , and  $bb'$  ones in the  $t'$  case. As expected, we solved for the common masses  $m_{b'} = (2.7 \pm 0.1)$  and  $m_{t'} \approx 200$  TeV from the above channels, which should be solid and convincing. Such superheavy quarks with the huge Yukawa couplings form bound states. The contributions from the  $\bar{b}'b'$  scalars to Higgs boson production via gluon fusion were assessed in an effective approach. Employing the eigenfunctions for scalar bound states in a Yukawa potential available in the literature, we calculated the widths appearing in the Breit-Wigner propagator associated with the scalars. We further fixed the relevant effective couplings for the gluon-gluon-scalar vertices and for the new scalar transition to a Higgs boson. The new scalar contributions at the scale of the Higgs boson mass turned out to be of  $O(10^{-3})$  of the top-quark one in the SM at most and is negligible. This estimate illustrated why these superheavy quarks could bypass the current experimental constraints from Higgs boson production via gluon fusion and decay to photon pairs and why one should continue the search for fourth generation  $b'$  quarks or their resonances at the (high-luminosity) Large Hadron Collider.

## ACKNOWLEDGMENTS

We thank K. F. Chen, Y. T. Chien, X. G. He, W. S. Hou, and P. Q. Hung for stimulating discussions. This work was supported in part by National Science and Technology Council of the Republic of China under Grant No. MOST-110-2112-M-001-026-MY3.

## APPENDIX: DERIVATION OF THE DISPERSION RELATION AND ITS SOLUTION

We recapture the derivation of the dispersion relation in Eq. (5) and of its solution in Eq. (6) for a self-contained presentation. Express the mixing amplitude for the neutral states  $Q\bar{u}$  and  $\bar{Q}u$  as

$$\begin{aligned} \mathcal{A}(m_Q) = & \sum_{i,j} \lambda_i \lambda_j [(M_{ij}(m_Q) + i\Gamma_{ij}(m_Q)) \bar{v}_i \gamma^\mu (1 - \gamma_5) \\ & \times u_Q \bar{u}_i \gamma_\mu (1 - \gamma_5) v_{\bar{Q}} + (M'_{ij}(m_Q) \\ & + i\Gamma'_{ij}(m_Q)) \bar{v}_i (1 - \gamma_5) u_Q \bar{u}_i (1 - \gamma_5) v_{\bar{Q}}], \quad (\text{A1}) \end{aligned}$$

where  $m_Q$  is the mass of the heavy quark  $Q$ , the light quark  $u$  is assumed to be massless for simplicity,  $\lambda_i \equiv V_{Qi}^* V_{ui}$  are the products of the CKM matrix elements,  $u_Q, v_{\bar{Q}}, \dots$  represent the quark spinors, the first (second) term on the right-hand side denotes the  $(V-A)(V-A)$   $[(S-P)(S-P)]$  structure, and  $M_{ij}^{(r)}$  ( $\Gamma_{ij}^{(r)}$ ) collects the real (imaginary) piece of the amplitude.

Since the last line in Eq. (3) contains an odd power of  $1/m_Q$ , the construction of a dispersion relation should begin with the contour integration in the complex  $m$  plane, instead of the  $m^2$  plane, which possesses different branching cuts. The designated contour has been described in Sec. II and depicted in Fig. 1. As stated in Sec. II, we focus on the  $(V-A)(V-A)$  contribution, and consider the contour integrations of the modified amplitudes

$$\Pi_{ij}(m) \equiv F_{ij}(m)[M_{ij}(m) + i\Gamma_{ij}(m)], \quad (\text{A2})$$

where the functions  $F_{ij}(m)$  have been defined in Eq. (4),

$$\begin{aligned} F_{db}(m) &= \frac{m^4}{(m^2 - m_b^2)^2}, \\ F_{sb}(m) &= \frac{m^4}{[m^2 - (m_b + m_s)^2]^2 \sqrt{m^2 - (m_b - m_s)^2}^3}, \\ F_{bb}(m) &= \frac{m}{m^2 - 4m_b^2}. \quad (\text{A3}) \end{aligned}$$

The analytical properties of the above amplitudes in the  $m$  plane have been discussed in Sec. II.

We have the identity

$$\frac{1}{2\pi i} \oint \frac{\Pi_{ij}(m)}{m - m_Q} dm = 0, \quad (\text{A4})$$

which vanishes, for the contour encloses unphysical regions and residues of potential poles at low  $m$  have been suppressed by  $F_{ij}(m)$  in Eq. (A3). The contribution along the small clockwise circle in Fig. 1 yields  $\text{Re}\Pi_{ij}(m_Q)$ , and those from the four horizontal sections lead to the dispersive integrals of  $\text{Im}\Pi_{ij}(m)$ . Equation (A4) is rewritten as

$$\begin{aligned} \text{Re}\Pi_{ij}(m_Q) = & \frac{1}{\pi} \int_{M_{ij}}^R \frac{\text{Im}\Pi_{ij}(m)}{m - m_Q} dm - \frac{1}{\pi} \int_{-R}^{-M_{ij}} \frac{\text{Im}\Pi_{ij}(m)}{m - m_Q} dm \\ & + \frac{1}{2\pi i} \int_{C_R} \frac{\Pi_{ij}^{\text{box}}(m)}{m - m_Q} dm, \quad (\text{A5}) \end{aligned}$$

with the hadronic threshold  $M_{ij}$ . The unknown function  $\text{Im}\Pi_{ij}(m)$  acquires nonperturbative contributions from the small  $m$  region. The integrand  $\Pi_{ij}(m)$ , taking values along the large counterclockwise circle  $C_R$ , can be reliably replaced by the perturbative one  $\Pi_{ij}^{\text{box}}(m)$ .

The real part  $\text{Re}\Pi_{ij}^{\text{box}}$  and the imaginary part  $\text{Im}\Pi_{ij}^{\text{box}}$  of the box-diagram contribution respect the dispersion relation

$$\begin{aligned} \text{Re}\Pi_{ij}^{\text{box}}(m_Q) = & \frac{1}{\pi} \int_{m_{ij}}^R \frac{\text{Im}\Pi_{ij}^{\text{box}}(m)}{m - m_Q} dm - \frac{1}{\pi} \int_{-R}^{-m_{ij}} \\ & \times \frac{\text{Im}\Pi_{ij}^{\text{box}}(m)}{m - m_Q} dm + \frac{1}{2\pi i} \int_{C_R} \frac{\Pi_{ij}^{\text{box}}(m)}{m - m_Q} dm, \quad (\text{A6}) \end{aligned}$$

because of the analyticity,  $m_{ij}$  in the first two integrals on the right-hand side being the quark-level threshold. We equate  $\text{Re}\Pi_{ij}(m_Q)$  and  $\text{Re}\Pi_{ij}^{\text{box}}(m_Q)$ , i.e., Eqs. (A5) and (A6) at large enough  $m_Q \gg M_{ij}$ , where perturbative evaluations are reliable, arriving at

$$\begin{aligned} & \int_{M_{ij}}^R \frac{\text{Im}\Pi_{ij}(m)}{m - m_Q} dm - \int_{-R}^{-M_{ij}} \frac{\text{Im}\Pi_{ij}(m)}{m - m_Q} dm \\ & = \int_{m_{ij}}^R \frac{\text{Im}\Pi_{ij}^{\text{box}}(m)}{m - m_Q} dm - \int_{-R}^{-m_{ij}} \frac{\text{Im}\Pi_{ij}^{\text{box}}(m)}{m - m_Q} dm. \quad (\text{A7}) \end{aligned}$$

The contributions from the large circle  $C_R$  on the two sides have been canceled. The modified amplitudes  $\text{Im}\Pi_{ij}(m)$  and  $\text{Im}\Pi_{ij}^{\text{box}}(m)$  are even functions of  $m$ . Hence, we apply the variable change  $m \rightarrow -m$  to the second integrals on both sides of Eq. (A7), which then reduces to Eq. (1) in the standard form with the integration variable  $m^2$ .

The variable changes  $m_Q^2 - m_{ij}^2 = u\Lambda$  and  $m^2 - m_{ij}^2 = v\Lambda$ , with  $\Lambda$  being an arbitrary scale, turn Eq. (5) into

$$\int_0^\infty dv \frac{\Delta\rho_{ij}(v)}{u - v} = 0. \quad (\text{A8})$$

Since  $\Delta\rho_{ij}(v)$  diminishes at large  $v$ , namely, the major contribution to Eq. (A8) comes from the region with finite  $v$ , we expand Eq. (A8) into a power series in  $1/u$  for sufficiently large but still arbitrary  $u$  by inserting  $1/(u - v) = \sum_{i=k}^\infty v^{k-1}/u^k$ . Equation (A8) thus demands a vanishing coefficient for every power of  $1/u$ . We start with the case with  $N$  vanishing coefficients,

$$\int_0^\infty dv v^{k-1} \Delta\rho_{ij}(v) = 0, \quad k = 1, 2, 3 \dots, N, \quad (\text{A9})$$

where  $N$  will be extended to infinity eventually. The first  $N$  generalized Laguerre polynomials  $L_0^{(\alpha)}(v), L_1^{(\alpha)}(v), \dots, L_{N-1}^{(\alpha)}(v)$  are composed of the terms  $1, v, \dots, v^{N-1}$  appearing in the above expressions. Therefore, Eq. (A9) implies an expansion of  $\Delta\rho_{ij}(v)$  in terms of  $L_k^{(\alpha)}(v)$  with degrees  $k$  not lower than  $N$ ,

$$\Delta\rho_{ij}(v) = \sum_{k=N}^{N_{ij}} a_{ij}^{(k)} v^{\alpha_{ij}} e^{-v} L_k^{(\alpha_{ij})}(v), \quad N_{ij} > N, \quad (\text{A10})$$

owing to the orthogonality of the polynomials, in which  $a_{ij}^{(k)}$  represent a set of unknown coefficients. The index  $\alpha_{ij}$  describes the behavior of  $\Delta\rho_{ij}(v)$  around  $v \sim 0$ . The highest degree  $N_{ij}$  can be fixed, in principle, by the initial condition  $-\text{Im}\Pi_{ij}^{\text{box}}(v)$  of  $\Delta\rho_{ij}(v)$  in the interval  $(0, (M_{ij}^2 - m_{ij}^2)/\Lambda)$  of  $v$ . Because  $-\text{Im}\Pi_{ij}^{\text{box}}(v)$  is a smooth function,  $N_{ij}$  needs not be infinite.

A generalized Laguerre polynomial takes the approximate form for large  $k$ ,  $L_k^{(\alpha)}(v) \approx k^{\alpha/2} v^{-\alpha/2} e^{v/2} J_\alpha(2\sqrt{kv})$  [42], up to corrections of  $1/\sqrt{k}$ . Equation (A10) becomes

$$\Delta\rho_{ij}(m) \approx \sum_{k=N}^{N_{ij}} a_{ij}^{(k)} \sqrt{\frac{k(m^2 - m_{ij}^2)^{\alpha_{ij}}}{\Lambda}} e^{-(m^2 - m_{ij}^2)/(2\Lambda)} \times J_{\alpha_{ij}} \left( 2\sqrt{\frac{k(m^2 - m_{ij}^2)}{\Lambda}} \right), \quad (\text{A11})$$

where  $v = (m^2 - m_{ij}^2)/\Lambda$  has been inserted. Defining the scaling variable  $\omega \equiv \sqrt{N/\Lambda}$ , we have the approximation  $N_{ij}/\Lambda = \omega^2 [1 + (N_{ij} - N)/N] \approx \omega^2$  for finite  $N_{ij} - N$ . The common Bessel functions  $J_{\alpha_{ij}}(2\sqrt{k(m^2 - m_{ij}^2)/\Lambda}) \approx J_{\alpha_{ij}}(2\omega\sqrt{m^2 - m_{ij}^2})$  for  $k = N, N+1, \dots, N_{ij}$  can be factored out, such that the unknown coefficients are summed into a single parameter  $y_{ij} = \sum_{k=N}^{N_{ij}} a_{ij}^{(k)}$ . We are allowed to treat  $\omega$  as a finite variable, though both  $N$  and  $\Lambda$  can be arbitrarily large. The arbitrariness of  $\Lambda$ , which traces back to that of the large circle radius  $R$ , goes into the variable  $\omega$ . The exponential suppression factor  $e^{-(m^2 - m_{ij}^2)/(2\Lambda)} = e^{-\omega^2(m^2 - m_{ij}^2)/(2N)}$  is further replaced by unity for finite  $\omega$  and large  $N$ . Equation (A11) then gives the solution in Eq. (6).

- 
- [1] H. n. Li, *Phys. Rev. D* **107**, 094007 (2023).  
[2] H. n. Li, *Phys. Rev. D* **108**, 054020 (2023).  
[3] H. n. Li, arXiv:2306.03463.  
[4] H. n. Li, H. Umeeda, F. Xu, and F. S. Yu, *Phys. Lett. B* **810**, 135802 (2020).  
[5] H. n. Li and H. Umeeda, *Phys. Rev. D* **102**, 094003 (2020).  
[6] H. n. Li and H. Umeeda, *Phys. Rev. D* **102**, 114014 (2020).  
[7] A. S. Xiong, T. Wei, and F. S. Yu, arXiv:2211.13753.  
[8] B. Belfatto and Z. Berezhiani, *J. High Energy Phys.* **08** (2023) 162.  
[9] A. Santamaria, *Phys. Lett. B* **305**, 90 (1993).  
[10] B. Holdom, *Phys. Rev. Lett.* **57**, 2496 (1986); **58**, 177(E) (1987); W. A. Bardeen, C. T. Hill, and M. Lindner, *Phys. Rev. D* **41**, 1647 (1990); C. T. Hill, M. A. Luty, and E. A. Paschos, *Phys. Rev. D* **43**, 3011 (1991); T. Elliott and S. F. King, *Phys. Lett. B* **283**, 371 (1992).  
[11] Y. Mimura, W. S. Hou, and H. Kohyama, *J. High Energy Phys.* **11** (2013) 048.  
[12] S. W. Ham, S. K. Oh, and D. Son, *Phys. Rev. D* **71**, 015001 (2005); M. S. Carena, A. Megevand, M. Quiros, and C. E. M. Wagner, *Nucl. Phys.* **B716**, 319 (2005); R. Fok and G. D. Kribs, *Phys. Rev. D* **78**, 075023 (2008); Y. Kikukawa, M. Kohda, and J. Yasuda, *Prog. Theor. Phys.* **122**, 401 (2009).  
[13] W. S. Hou, *Chin. J. Phys.* **47**, 134 (2009).  
[14] N. Chen and H. J. He, *J. High Energy Phys.* **04** (2012) 062; O. Eberhardt, G. Herbert, H. Lacker, A. Lenz, A. Menzel, U. Nierste, and M. Wiebusch, *Phys. Rev. Lett.* **109**, 241802 (2012); A. Djouadi and A. Lenz, *Phys. Lett. B* **715**, 310 (2012); E. Kuflik, Y. Nir, and T. Volansky, *Phys. Rev. Lett.* **110**, 091801 (2013).  
[15] H. J. He, N. Polonsky, and S. f. Su, *Phys. Rev. D* **64**, 053004 (2001).  
[16] P. Q. Hung and C. Xiong, *Nucl. Phys.* **B847**, 160 (2011).  
[17] T. Enkhbat, W. S. Hou, and H. Yokoya, *Phys. Rev. D* **84**, 094013 (2011).  
[18] P. Q. Hung and C. Xiong, *Nucl. Phys.* **B848**, 288 (2011).  
[19] D. Das, A. Kundu, and I. Saha, *Phys. Rev. D* **97**, 011701 (2018).  
[20] H. n. Li, *Phys. Rev. D* **107**, 054023 (2023).  
[21] A. A. Petrov, *Phys. Rev. D* **56**, 1685 (1997).  
[22] H. Y. Cheng, *Phys. Rev. D* **26**, 143 (1982).  
[23] A. J. Buras, W. Slominski, and H. Steger, *Nucl. Phys.* **B245**, 369 (1984).  
[24] G. Buchalla, A. J. Buras, and M. E. Lautenbacher, *Rev. Mod. Phys.* **68**, 1125 (1996).  
[25] M. A. Shifman, A. I. Vainshtein, and V. I. Zakharov, *Nucl. Phys.* **B147**, 385 (1979); **B147**, 448 (1979).  
[26] T. Zhong, Z. H. Zhu, H. B. Fu, X. G. Wu, and T. Huang, *Phys. Rev. D* **104**, 016021 (2021).

- [27] A. Bazavov *et al.* (Fermilab Lattice, MILC and TUMQCD Collaborations), *Phys. Rev. D* **98**, 054517 (2018).
- [28] R. L. Workman *et al.* (Particle Data Group), *Prog. Theor. Exp. Phys.* **2022**, 083C01 (2022).
- [29] A. Deur, S. J. Brodsky, and G. F. de Teramond, *Prog. Part. Nucl. Phys.* **90**, 1 (2016).
- [30] W. S. Hou, *Phys. Rev. D* **86**, 037701 (2012).
- [31] M. Napsuciale and S. Rodríguez, *Prog. Theor. Exp. Phys.* **2021**, 073B03 (2021).
- [32] L. H. Thomas, *Phys. Rev.* **47**, 903 (1935).
- [33] S. M. Ikhdaïr, *Central Eur. J. Phys.* **10**, 361 (2012).
- [34] J. P. Lansberg and T. N. Pham, *Phys. Rev. D* **79**, 094016 (2009).
- [35] H. M. Georgi, S. L. Glashow, M. E. Machacek, and D. V. Nanopoulos, *Phys. Rev. Lett.* **40**, 692 (1978).
- [36] M. Spira, A. Djouadi, D. Graudenz, and P. M. Zerwas, *Nucl. Phys.* **B453**, 17 (1995).
- [37] I. Rosell, A. Pich, and J. J. Sanz-Cillero, *Nucl. Part. Phys. Proc.* **343**, 130 (2024).
- [38] R. N. Cahn and S. Dawson, *Phys. Lett.* **136B**, 196 (1984); K. Hikasa, *Phys. Lett.* **164B**, 385 (1985); G. Altarelli, B. Mele, and F. Pitolli, *Nucl. Phys.* **B287**, 205 (1987); T. Han, G. Valencia, and S. Willenbrock, *Phys. Rev. Lett.* **69**, 3274 (1992).
- [39] A. Tumasyan *et al.* (CMS Collaboration), *J. High Energy Phys.* **07** (2023) 219.
- [40] ATLAS Collaboration, Measurement of the total and differential cross-sections of  $t\bar{t}W$  production in  $pp$  collisions at 13 TeV with the ATLAS detector, Report No. ATLAS-CONF-2023-019.
- [41] A. C. Canbay and O. Cakir, *Phys. Rev. D* **108**, 095006 (2023).
- [42] D. Borwein, J. M. Borwein, and R. E. Crandall, *SIAM J. Numer. Anal.* **46**, 3285 (2008).